LONDON'S GLOBAL UNIVERSITY

Numerical Approximations of the Inverse $\mathbb{Z}$-Transform

Final Year Project Report

Roman Ryan Karim[1]

Dr Carolyn Phelan

Department of Computer Science
University College London

Submission date: May 6, 2024

[1]**Disclaimer:** This report is submitted as part requirement for the MEng degree in Mathematical Computation at UCL. It is substantially the result of my own work except where explicitly indicated in the text. The report may be freely copied and distributed provided the source is explicitly acknowledged.

Abstract

Contents

Chapter 1

Introduction

1.1 Motivation

1.2 Aims and Objectives

1.3 Overview

In Chapter 2, we provide a self-contained technical background on the key concepts and methods used in this project. Given the breadth of the topic, references are included for those looking to delve deeper into the subject.

In Chapter 3, we outline the experiments conducted in Chapter 4 to evaluate the performance of the numerical approximation methods. We detail the implementation of the methods and the experimental setup, including parameter selection and the benchmarking process We then provide the results on a list of transform pairs and discuss the implications of the findings.

In Chapter 5, we summarize the findings of the project and discuss potential avenues for future work. This allows for ...

Chapter 2

Background

In Chapter 2, we establish a foundational understanding of the topic in hand. This section is designed to be self-contained, providing essential background for all readers, while references are included for those seeking a deeper exploration.

We conduct an analysis into the mathematical concepts used in option pricing, with a focus on Fourier-based methods. While a large body of theoretical work exists in this area, the practical implementation of these methods is often computationally expensive, especially when evaluating high-dimensional integrals involved in the pricing formulas. We study literature on numerical approximation methods and the application in the pricing of exotic options, specifically lookback and barrier options. Subsequently, we explore the use-case of machine learning techniques to optimize parameters during our experimentation in Chapter 3.

2.1 The $\mathcal{Z}$-Transform

The z-transform is a transformation of a real or complex time function $x(n)$, often used for analyzing discrete-time signals and systems. It is a generalization of the discrete-time Fourier transform (DTFT) that extends the analysis to the complex plane. The Z-transform is formally defined as:

$$X(z) = \mathcal{Z}_{n\to z}[x(n)] = \sum_{n=-\infty}^{\infty} x(n)z^{-n} \tag{2.1}$$

"By definition, a complex number z is an ordered pair (x, y) of real numbers x and y, written $z = (x, y)$" (Kreyszig, 2010). In practice, complex numbers are written in the form $z = x + iy$, where x and y are real numbers and i is the imaginary unit. We may find it easier to represent complex numbers in their polar form, $z = re^{i\theta}$, where r represents the magnitude of z and θ represents the angle of z with respect to the positive real axis.

In the analysis of causal systems - systems for which a time origin is defined and is illogical to consider signal values for negative time - the unilateral z-transform is used. Unlike the bilateral z-transform in Eq. (2.1), we sum from zero to positive infinity yielding

$$X(z) = \mathcal{Z}_{n\to z}[x(n)] = \sum_{n=0}^{\infty} x(n)z^{-n} \tag{2.2}$$

The region within the complex z-plane where the z-transform converges is known as the Region of Convergence (ROC). The ROC is defined for the set of values of z for which the z-transform is absolutely summable

$$\textbf{ROC} = \left\{ z : \sum_{n=0}^{\infty} |x(n)z^{-n}| < \infty \right\} \tag{2.3}$$

For causal sequences, the ROC is typically the exterior of the outermost pole in the Z-plane, denoted as $|z| > a$. If we say that z_1 converges, then z_1 exists within the ROC. Thus, all z such that $|z| \geq |z_1|$ also converge. This region excludes the poles themselves, as the transform does not converge at those points. For the system to be *stable*, the ROC must include the unit circle, $|z| = 1$, implying that all poles must lie within the unit circle (Loveless and Germano, 2021).

Example 1 *Consider the function given by*

keep here or in background?

$$H(z) = \frac{(z-i)(z+i)}{\left(z - \left(-\frac{1}{4} - \frac{1}{2}i\right)\right)\left(z - \left(\frac{1}{2} + \frac{1}{2}i\right)\right)} \tag{2.4}$$

The ROC of $H(z)$ must exclude the poles at $z = -\frac{1}{4} - \frac{1}{2}i$ and $z = \frac{1}{2} + \frac{1}{2}i$, thus the ROC is $|z| > \frac{1}{2}$. The system is stable as the ROC includes the unit circle.

2.1.1 Relation to the Fourier Transform

It is useful to note the relationship between the z-transform and the Fourier transform. Taking the Fourier transform of a sampled function $x(t)$ results in:

$$\mathcal{F}\left[x(t) \sum_{n=-\infty}^{\infty} \delta(t - n\Delta t)\right] = \int_{-\infty}^{\infty} x(t) \sum_{n=-\infty}^{\infty} \delta(t - n\Delta t) e^{-i\omega t} dt \tag{2.5}$$

$$= \sum_{n=-\infty}^{\infty} \int_{-\infty}^{\infty} x(t)\delta(t - n\Delta t) e^{-i\omega t} dt \tag{2.6}$$

$$= \sum_{n=-\infty}^{\infty} x(n\Delta t) e^{-i\omega n t} \tag{2.7}$$

where we make use of the sifting property of the delta function. If we normalize the sampling interval to 1, we get

$$\sum_{n=-\infty}^{\infty} x(n) e^{-in\omega} \tag{2.8}$$

This is the discrete-time Fourier transform (DTFT) of the sequence $x(n)$. The sequence $x(n)$ is sampled at discrete-time intervals $t_n = n\triangle t$, where the sampling interval $\triangle t$ is the time between consecutive samples and the time index n numbers the samples. The DTFT is a periodic function of ω with period 2π, and its existence relies on the absolute summability of the sequence $x(n)$:

$$\sum_{n=-\infty}^{\infty} |x(n)| < \infty \tag{2.9}$$

The Z-transform generalizes Eq. (2.8) to the complex plane, not just the unit circle where $r = 1$ (Schafer and Oppenheim, 1989).

2.1.2 Relation to Probability Distribution Functions

Random events and signals refer to situations where the outcome is not deterministic, but can be described by probability. Understanding these concepts involves using Probability Distribution Functions; the Probability Mass Function (PMF) for discrete random variables and the Probability Density Function (PDF) for continuous random variables. Given the nature of this project, we'll be focusing our attention on the PMF.

The PMF is defined for a discrete random variable X taking on values x_i with probabilities p_i, as $P(X = x_i) = p_i$. The PMF satisfies the following properties:

$$\sum_{i=0}^{n} p_i = 1 \qquad \text{and} \qquad 0 \leq p_i \leq 1 \ \forall i \tag{2.10}$$

We may find it useful to provide a concise representation of the entire distribution such that we expand upon the PMF, $p(x)$, to obtain the Probability Generating Function (PGF), $G_X(q)$, defined as

$$G_X(q) = E[q^X] = \sum_{x=0}^{\infty} p(x)q^x, \tag{2.11}$$

where $E[\cdot]$ denotes the expectation operator, and q is a complex number. We deliberately use q to distinguish the PGF from the z-transform (Eqn. 2.1).

Example 2 *Consider a fair six-sided dice. The PMF for the dice roll is given by*

$$p(x) = \begin{cases} \frac{1}{6} & \text{if } x = 1, 2, 3, 4, 5, 6 \\ 0 & \text{otherwise} \end{cases} \tag{2.12}$$

where $p(x)$ is the probability of rolling a number x. The PGF for the dice roll is then

$$G_X(q) = \sum_{x=0}^{\infty} p(x)q^x = \frac{1}{6}\sum_{x=1}^{6} q^x = \frac{q}{6} \cdot \frac{1 - q^6}{1 - q}, \tag{2.13}$$

where we use the formula for the sum of a geometric series. The PGF encapsulates the entire distribution of the dice roll into a single function.

The concept of summarizing information is not unique to probability theory. In the analysis of signals, we aim to encapsulate the behaviour of a sequence into a single function. This is akin to the PGF, where the z-transform is used to analyze discrete-time signals and systems. Drawing on the principles outlined by Ross (2014), we can bridge the gap between probability theory and signal processing, leveraging the z-transform to analyze the behaviour of signals in the complex plane.

2.2 The Inverse $\mathcal{Z}$-Transform

The inverse Z-transform aims to find the n-th value of the sequence $x(n)$ given the Z-transform $X(z)$. This is commonly defined as a Cauchy integral around a contour C in the complex plane. The contour C is a counter-clockwise closed path that encloses the region of convergence (ROC). The inverse Z-transform is formally given by

$$x(n) = \mathcal{Z}^{-1}_{z\to n}[X(z)] = \frac{1}{2\pi i}\oint_C X(z)z^{n-1}dz \tag{2.14}$$

In practical settings, numerical approximations are often used due to the computational challenges of evaluating the Cauchy integral. Whilst there are many ways to go about this (Merrikh-Bayat, 2014; Rajković et al., 2004; Horváth et al., 2020), most methods are done on a circular contour. Aligning with the focus of our project, we shift our attention to contour integrals.

2.2.1 Abate and Whitt 1992

The numerical approximation formula offered by Abate and Whitt (1992a,b) is based on a Fourier series catering to the inversion of probability generating functions as elucidated in Section 2.1.2. The format is conducive to queuing theory and other probabilistic models where the Z-transform is defined as $q = 1/z$. The authors approximate the inversion using a trapezoidal rule for numerical integration over a complex contour given by

$$x(n) \approx \frac{1}{2nr^n}\left(X(r) + 2\sum_{k=1}^{n-1}(-1)^k \mathrm{Re}\left(X(re^{\frac{ik\pi}{n}})\right) + (-1)^n X(-r)\right) \tag{2.15}$$

The parameter r is used to control the error; setting $r = 10^{-\lambda/2n}$ yields an accuracy bound of $10^{-\lambda}$. The authors leverage the inherent symmetry within the complex plane to enhance computational efficiency by exploiting the complex conjugate symmetry of $X(z)$; each term $X(re^{\frac{ik\pi}{n}})$ in the upper half has a mirror image in the lower half. The computational load is thus halved by *folding* the problem in this manner.

Given the nature of this project, we may find it easier to use the following definition, where we set $z = 1/q$, to approximate Eq. (2.14).

$$x(n) \approx \frac{1}{2nr^n}\left(X(\frac{1}{r}) + 2\sum_{k=1}^{n-1}(-1)^k \mathrm{Re}\left(X(\frac{1}{re^{\frac{ik\pi}{n}}})\right) + (-1)^n X(-\frac{1}{r})\right) \tag{2.16}$$

The Nyquist-Shannon sampling theorem states that a signal must be sampled at a rate of at least twice the highest frequency present in the signal to avoid aliasing (Shannon, 1949; Nyquist, 1928). The number of points, n, used in Eqn. (2.16) must be sufficient to capture the information properly. If n is too small, the approximation may lead to inaccuracies - akin to aliasing in signal processing.

2.2.2 Cavers 1978

Extending upon our analysis in Section 2.1.1, Cavers (1978) proposes to sample the z-transform of a function on a circular contour at equally spaced points and then apply the inverse FFT to these sampled points to approximate the original time-domain signal. We can formulate this as:

$$f(n) = r^n \mathrm{IFFT}[f(re^{2\pi i/N})], \tag{2.17}$$

where r is the radius of the circular contour, n is the time index, and N is the number of points used in the DFT. The factor r^n scales the result appropriately based on the radius of the contour.

2.2.3 Series acceleration techniques

if we have time, otherwise remove this section

2.3 Optimization Techniques

In the context of computational mathematics, optimizations techniques are used to identify the optimal or a sufficiently effective solution to a problem within a given set of constraints. The goal is to minimize or maximize a specific objective function by systematically choosing the values of the variables. The objective function is often referred to as the *cost function* or *loss function* and the variables are referred to as *parameters*. The optimization problem can be formulated as

$$\text{minimize } f(x) \text{ subject to } x \in \Omega, \tag{2.18}$$

where $f(x)$ is the objective function and Ω is the feasible region defined by the constraints of the problem.

Gradient descent is one of the most popular algorithms for parameter optimization with success in Deep Learning and Neural Networks employing variants of the algorithm (Lu and Jin, 2017; Zhang, 2019; Zeebaree et al., 2019). The adaptability to diverse problem domains (Tian et al., 2023) parallels our use case, where gradient descent is applied outside traditional deep learning to optimize parameters of a mathematical function (Persson et al., 2022).

2.3.1 Gradient Descent

Gradient descent iteratively converges to a local minimum of a function by moving in the direction of the steepest descent, as defined by the negative gradient. This method is expressed mathematically as

$$x_{k+1} = x_k - \alpha_k \nabla f(x_k), \tag{2.19}$$

where x_k is the parameter vector at iteration k, α_k is the learning rate, and $\nabla f(k)$ represents the gradient of the function at x_k. The selection of α_k determines the size of the step taken towards the minimum; too large can overshoot the minimum, too small can result in a long convergence time. The process repeats until a predetermined termination criterion is met, typically when the change in the value of $f(k)$ falls below a threshold. This iterative process is showcased in the pseudocode below:

Algorithm 1 Gradient Descent

```
Initialize x_0, set k = 0
while termination conditions not met do
    Compute gradient ∇f(x_k)
    Choose a suitable step size α_k
    Update x_{k+1} = x_k − α_k ∇f(x_k)
    k = k + 1
end while
```

Stochastic Gradient Descent

However, classic Gradient Descent faces limitations, including susceptibility to local minima and potential for overshooting or long convergence times. Stochastic Gradient Descent (SGD) addresses these issues by introducing variability in the optimization process. It modifies Eq. (2.19) to use a randomly selected subset of data to compute the gradient, to allow for dynamic adjustment of the learning rate and leveraging noise to escape local minima. We define the update rule to

$$x_{k+1} = x_k - \alpha_k \nabla f_{i_k}(x_k) \tag{2.20}$$

where $\nabla f_{i_k}(x_k)$ is the gradient of the cost function with respect to a random subset i_k. We thus avoid the pitfalls associated with a static learning rate and promote a quicker convergence time.

2.4 Option Pricing

The concept involves determining the value of options, which are financial contracts that give the holder the right, *but not the obligation*, to buy or sell an asset at a set price within a specified time-frame. The value of an option is derived from the underlying asset, which can be a stock, bond, or commodity.

A pivotal point in option pricing was the introduction of Black and Scholes (1973)'s model in estimating the price of European-style options, which can only be exercised at the expiration date. The Black-Scholes model is based on the assumption that the price of the underlying asset follows a geometric Brownian motion in idealistic conditions. However, many options traded in real markets are American-style, allowing the holder to exercise the option at any time before the expiration date. This complicates the pricing process as it involves solving an *optimum stopping problem*. Merton (1973) extends the Black-Scholes model to American options by expressing the price as the solution to a free boundary problem. While Merton's work provided a theoretical foundation, solving the free boundary problem analytically is challenging. Instead, numerical methods such as binomial trees (Cox et al., 1979) and simulation-based methods (Longstaff and Schwartz, 2001) have been developed to price American options.

2.4.1 Discrete Monitoring

In most cases, the payoff of an option depends on the price of the underlying asset at discrete points in time rather than continuously. This is known as discrete monitoring. Two widely traded types of discretely monitored options are lookback and barrier options (Dadachanji, 2015). These options are classified as *exotic options* where the payoff is based on the path of the underlying asset price rather than just the price at expiration.

Lookback Options

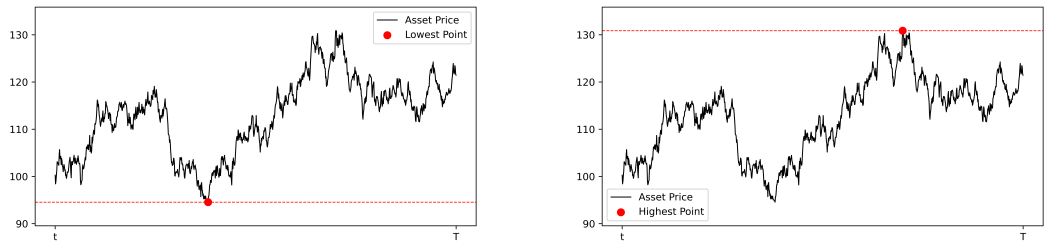

(a) Lookback Call Option

(b) Lookback Put Option

Figure 2.1: Illustration of Lookback Options: Displaying the mechanics of (a) Call Option and (b) Put Option. The red line represents the barrier, while the red dot marks the strike price.

The payoff depends on the maximum and minimum asset price over the life of the option. A *lookback call option* (Figure 2.1a) gives the holder the right to buy the asset at the lowest price during the option period, while a *lookback put option* (Figure 2.1b) allows the holder to sell the asset at the highest price during the option period.

Barrier Options

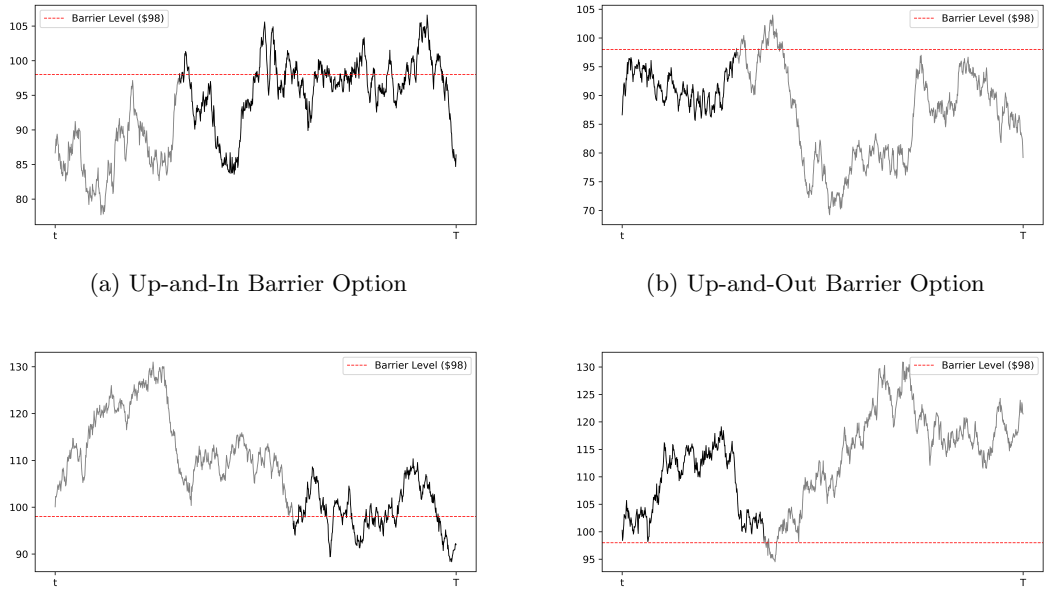

(a) Up-and-In Barrier Option

(b) Up-and-Out Barrier Option

(c) Down-and-In Barrier Option

(d) Down-and-Out Barrier Option

Figure 2.2: Illustration of Barrier Options: Displaying the active (black) and inactive (grey) phases of each option type. (a) Up-and-In Option, (b) Up-and-Out Option (c) Down-and-In Option, and (d) Down-and-Out Option. The red line represents the barrier.

The payoff depends on whether the price of the underlying asset reaches a certain level (the barrier) during the life of the option. A *knock-in* barrier option only come into existence if the barrier has been touched, while a *knock-out* barrier option ceases to exist instead. For example, a *down-and-out* barrier option (Figure 2.2d) is a type of knock-out option that becomes worthless if the price of the underlying asset falls below the barrier level. On the other hand, a *down-and-in* barrier option (Figure 2.2c) is a type of knock-in option that only becomes active if the asset price falls below the barrier level.

2.4.2 Modelling Asset Prices

2.4.3 Fourier-Based Pricing

However, the pricing of these options can be computationally expensive due to the high-dimensional integrals involved in the pricing formulas. Whilst Heston (1993) explored the idea of modelling asset prices in the Fourier domain, Carr and Madan (1999) were the first to price European options expressing both the characteristic function and the payoff in the Fourier domain. It involved transforming the pricing problem from the time domain to the frequency domain, where the pricing formula simplifies to a one-dimensional integral. The Fourier-based methods have been widely used for the pricing of options discussed in Section 2.4.1 (Eberlein et al., 2010).

Fang and Oosterlee (2009a) introduced a pricing technique based on the Fourier-cosine expansion approximating the characteristic function of the underlying asset price, which was then expanded to a broader class of exotic options (Fang and Oosterlee, 2009b, 2011) and general lévy processes (Lord et al., 2008). Whilst the method shows high levels of accuracy with exponential error convergence on the number of terms, this is only the case when the governing probability density function is sufficiently smooth. When modelling the asset price by the variance gamma process (Madan et al., 1998), we achieve only algebraic error convergence due to the discontinuities in the process. Ruijter et al. (2015) showed that this can be remedied using spectral filters however the issue remains in that the computational time is linearly dependent on the number of monitoring dates for discretely monitored options. This seems to also be the case for Feng and Linetsky (2008)'s employment of the Hilbert transform using backward induction to price barrier options.

In an effort to eliminate the computational inefficiency tied to the number of monitoring dates, Fusai et al. (2006) looked into shifting the pricing problems from the time domain into the z-domain, where convolution operations become straightforward multiplications. This helped set the stage for Fusai et al. (2016)'s method incorporating the Hilbert and z-transform to calculate the **Wiener-Hopf factors**, which decompose the characteristic function of the price process into two parts; positive and negative jumps. The authors demonstrated that the computational cost is independent of the number of monitoring dates, and the error decays exponentially with the number of grid points. Whilst extensions to the method have been made such as those by Phelan (2018)'s new scheme using spectral filters to improve convergence (Phelan et al., 2019), we shift our focus to the use-case of the inverse z-transform in the pricing of options.

2.4.4 NIZT in Option Pricing

- calculating characteristic function's z-transform - PD of asset's price
- IZT to get the PD of the asset's price at different points
- use of the PD to calculate the option price

Chapter 3

Experiment

Having established the theoretical foundation, we now turn our attention to the practical implementation of methods proposed by Abate and Whitt (1992a,b) and Cavers (1978). Whilst the former is based on a circular contour, we also explore the idea laid out by Boyarchenko and Levendorskiĭ (2022) in sampling the z-transform on a sinh-deformation.

This chapter outlines the experimental setup, implementation and evaluation of the methods. We measure our results in terms of accuracy and computational efficiency against well-known transformation pairs in an attempt to provide a thorough comparison of the methods to determine the most effective approach.

If we get series acceleration, include here asw

3.1 Circular Contour

"The inverse at point T can be obtained from the contour integral where C is a counter-clockwise closed path encircling the origin and entirely in the region of convergence" (Horváth et al., 2020). A circular contour is commonly used to solve Equation 2.14, defined as $z = re^{i\theta}$, such that r encloses the poles of the z-transform.

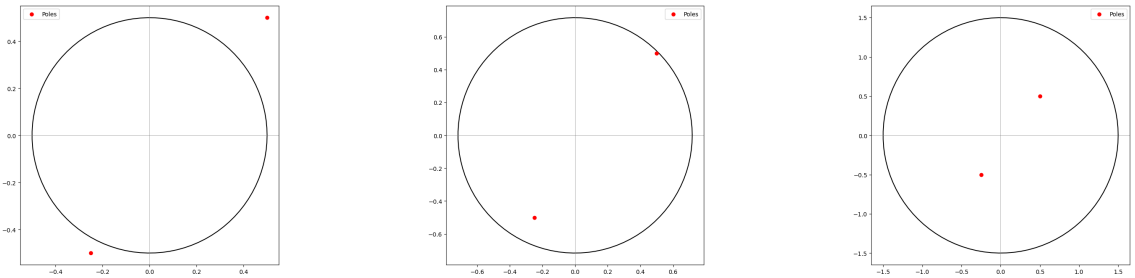

(a) r = 0.5 (b) r = 0.72 (2 d.p.) (c) r = 1.5

Figure 3.1: Displaying the effect of the radius r on a circular contour ($n = 100$). The red dots represent the poles of $H(z)$ in Example 1 with (a) including the poles within the ROC, (b) excluding the poles but inclusive of the unit circle, and (c) excluding the poles but not stable.

3.1.1 Abate and Whitt 1992

Algorithm 2 Implementation of Equation 2.16

procedure AbateWhitt($\tilde{f}, n$)
  $\lambda \leftarrow x_{\in}\mathbb{Z}^{+}$
  $\rho \leftarrow 10^{-\lambda/(2\cdot n)}$
  summation $\leftarrow 0$
  for $k \leftarrow 1$ **to** $n-1$ **do**
    $z \leftarrow \frac{1}{\rho\cdot\exp(\mathrm{i}\cdot k\cdot\pi/n)}$
    sum $\leftarrow$ sum $+ (-1)^k \cdot \mathrm{Re}(\tilde{f}(z))$
  end for
  sum $\leftarrow \tilde{f}(\frac{1}{\rho}) + 2\cdot$ sum $+ (-1)^n \cdot \tilde{f}(\frac{1}{-\rho})$
  return $\frac{\text{sum}}{2\cdot n\cdot\rho^n}$
end procedure

3.1.2 Cavers 1978

3.2 Sinh Deformation

A circular contour integral is commonly used for approximating the inverse z-transform as we've seen in Section 2.2.1 and 2.2.2. However, this does not mean it may be the best option. Boyarchenko and Levendorskiĭ (2022) propose a new method for a numerical evaluation of Equation 2.14 by deforming the commonly used circular contour $\{z = re^{i\theta} | -\pi < \theta < +\pi\}$ through the conformal mapping:

$$\xi(y) = \sigma + ib\sinh(i\theta + y), \tag{3.1}$$

where parameters are chosen such that $\sigma_{\in}\mathbb{R}$, $b > 0$, and θ is restricted to the interval $(-\pi/2, \pi/2)$. The unique selection of parameters allows the contour to be tailored specifically to the characteristics of $X(z)$. The authors state that the conformal mapping alleviates typical errors which are discussed in the relevant texts (Boyarchenko and Levendorskiĭ, 2014, 2019; Schmelzer and Trefethen, 2007). Applying a change of variables to Equation 2.14 yields

$$x(n) = \int_{\mathbb{R}} \frac{b}{2\pi}\xi(y)^{-n-1}\cosh(i\theta + y)X(\xi(y))dy. \tag{3.2}$$

By denoting the integrand as $f_n(y)$ and approximating the application of the infinite trapezoidal, we have

$$x(n) \approx 2\epsilon\ \mathrm{Re}\left(\sum_{j=0}^{M_0} f_n(j\epsilon)(1 - \delta_{j0}/2)\right) \tag{3.3}$$

need to look more into it

- mention sufficient conditions under which this works (next paper)
- talk about why he does this

3.2.1 Deforming the Contour

In an attempt to recreate the unit circle from the conformal mapping (3.1), we first try to understand the effects of the parameters on the contour. We plot the contour for different values of σ, b and y to observe the deformation.

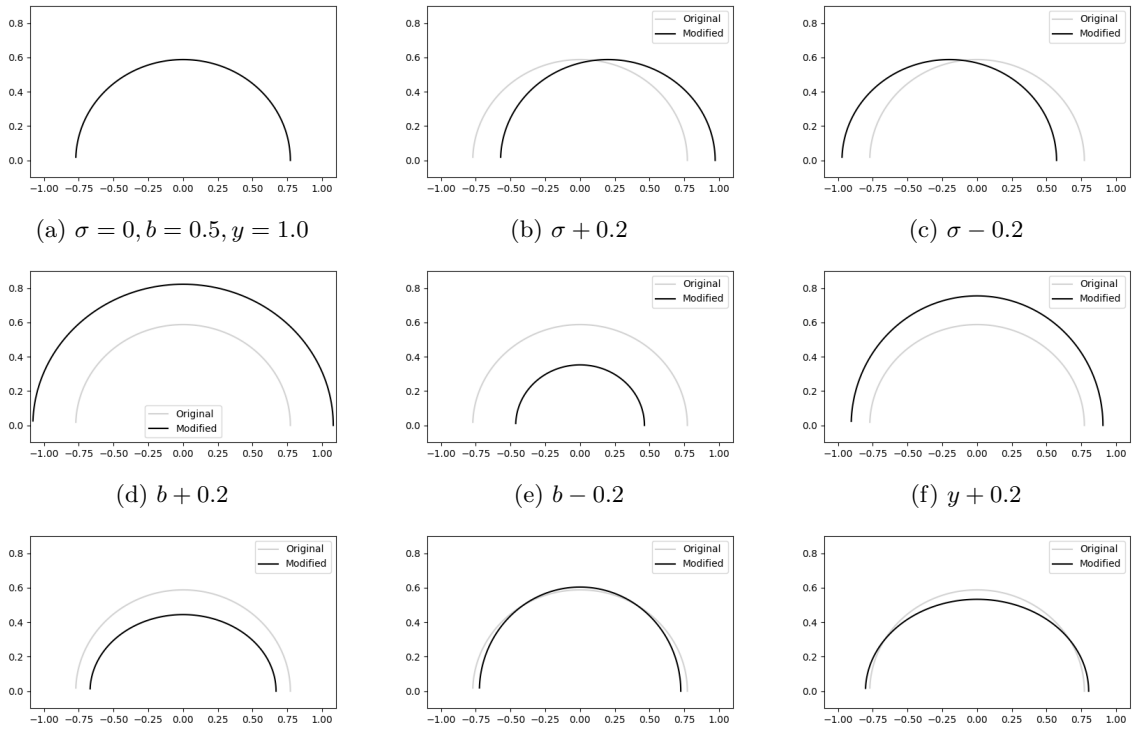

(a) $\sigma = 0, b = 0.5, y = 1.0$ (b) $\sigma + 0.2$ (c) $\sigma - 0.2$

(d) $b + 0.2$ (e) $b - 0.2$ (f) $y + 0.2$

(g) $y - 0.2$ (h) $b - 0.1, y + 0.2$ (i) $b + 0.1, y - 0.2$

Figure 3.2: Displaying the effect of the parameters on the contour for the conformal mapping (3.1) with $\{-\frac{\pi}{2} \leq \theta \leq \frac{\pi}{2}\}$ and $n = 100$ points. Plots (b, c, d, e, f, g, h, i) highlights the changes in parameter the effects on the contour in comparison to the base contour (a). The black line represents the created contour, with the grey contour representing the base contour with parameters $\sigma = 0, b = 0.5, y = 1.0$.

In relation to the base contour (Figure 3.2a), we observe that increasing σ shifts the contour to the right (Figure 3.2b), while decreasing σ shifts the contour to the left (Figure 3.2c). The parameter b acts as a scale factor on the sinh deformation as shown in Figure 3.2d and 3.2e. Similarly, y acts as a scale factor but with a more pronounced vertical effect as seen in Figure 3.2f and 3.2g. Mixing the parameters b and y results in a more complex deformation where the counter-opposing effects changes the contour in a non-linear manner (Figure 3.2h and 3.2i).

3.2.2 Parameter Grid Search

- use of grid search to find optimal parameters
- different search criteria's (*e.g. area, x-axis perimeter, etc*)
- might also be useful to try find parameters that give the results?
- use of SGD and loss function

3.3 Numerical Benchmarking

Function	$x(z)$	$X(z)$
Heaviside Step	1	$z/(z-1)$
Polynomial	t	$z/(z-1)^2$
Decaying Exp	e^{-at}	$1/(1-\exp(a\triangle t)z^{-1})$
Sinusoidal	$\sin(\omega t)$	$(z^{-1}\sin(w\triangle t))/(1-2z^{-1}\cos(w\triangle t)+z^{-2})$

Table 3.1: List of Transform Pairs

Chapter 4

Results

Chapter 5

Conclusion

5.1 Summary

5.2 Future Work

5.2.1 Parameter Selection

During the course of the project, there was no set method for selecting the parameters for Equation 3.1, hence, our effort of employing numerous techniques in an attempt to find the optimal parameters. However, as of recently at the time of writing, Boyarchenko and Levendorskiĭ (2024) have released a paper detailing parameter selection for the conformal mapping (3.1).

5.3 Acknowledgements

Bibliography

Abate, J. and Whitt, W. (1992a). The fourier-series method for inverting transforms of probability distributions. *Queueing systems*, 10:5–87.

Abate, J. and Whitt, W. (1992b). Numerical inversion of probability generating functions. *Operations Research Letters*, 12(4):245–251.

Black, F. and Scholes, M. (1973). The pricing of options and corporate liabilities. *Journal of political economy*, 81(3):637–654.

Boyarchenko, S. and Levendorskiĭ, S. (2014). Efficient variations of the fourier transform in applications to option pricing. *Journal of Computational Finance*, 18(2).

Boyarchenko, S. and Levendorskiĭ, S. (2019). Sinh-acceleration: Efficient evaluation of probability distributions, option pricing, and monte carlo simulations. *International Journal of Theoretical and Applied Finance*, 22(03):1950011.

Boyarchenko, S. and Levendorskiĭ, S. (2022). Efficient inverse z-transform and pricing barrier and lookback options with discrete monitoring. *arXiv preprint arXiv:2207.02858*.

Boyarchenko, S. and Levendorskiĭ, S. (2024). Efficient inverse z-transform and wiener-hopf factorization. *arXiv preprint arXiv:2404.19290*.

Carr, P. and Madan, D. (1999). Option valuation using the fast fourier transform. *Journal of computational finance*, 2(4):61–73.

Cavers, J. (1978). On the fast fourier transform inversion of probability generating functions. *IMA Journal of Applied Mathematics*, 22(3):275–282.

Cox, J. C., Ross, S. A., and Rubinstein, M. (1979). Option pricing: A simplified approach. *Journal of financial Economics*, 7(3):229–263.

Dadachanji, Z. (2015). *FX Barrier Options: A comprehensive guide for industry quants*. Springer.

Eberlein, E., Glau, K., and Papapantoleon, A. (2010). Analysis of fourier transform valuation formulas and applications. *Applied Mathematical Finance*, 17(3):211–240.

Fang, F. and Oosterlee, C. W. (2009a). A novel pricing method for european options based on fourier-cosine series expansions. *SIAM Journal on Scientific Computing*, 31(2):826–848.

Fang, F. and Oosterlee, C. W. (2009b). Pricing early-exercise and discrete barrier options by fourier-cosine series expansions. *Numerische Mathematik*, 114(1):27–62.

Fang, F. and Oosterlee, C. W. (2011). A fourier-based valuation method for bermudan and barrier options under heston's model. *SIAM Journal on Financial Mathematics*, 2(1):439–463.

Feng, L. and Linetsky, V. (2008). Pricing discretely monitored barrier options and defaultable bonds in lévy process models: a fast hilbert transform approach. *Mathematical Finance: An International Journal of Mathematics, Statistics and Financial Economics*, 18(3):337–384.

Fusai, G., Abrahams, I. D., and Sgarra, C. (2006). An exact analytical solution for discrete barrier options. *Finance and Stochastics*, 10:1–26.

Fusai, G., Germano, G., and Marazzina, D. (2016). Spitzer identity, wiener-hopf factorization and pricing of discretely monitored exotic options. *European Journal of Operational Research*, 251(1):124–134.

Heston, S. L. (1993). A closed-form solution for options with stochastic volatility with applications to bond and currency options. *The review of financial studies*, 6(2):327–343.

Horváth, I., Mészáros, A., and Telek, M. (2020). Numerical inverse transformation methods for z-transform. *Mathematics*, 8(4):556.

Kreyszig, E. (2010). *Advanced Engineering Mathematics*. John Wiley & Sons.

Longstaff, F. A. and Schwartz, E. S. (2001). Valuing american options by simulation: a simple least-squares approach. *The review of financial studies*, 14(1):113–147.

Lord, R., Fang, F., Bervoets, F., and Oosterlee, C. W. (2008). A fast and accurate fft-based method for pricing early-exercise options under lévy processes. *SIAM Journal on Scientific Computing*, 30(4):1678–1705.

Loveless, B. and Germano, G. (2021). Review of numerical inversion techniques of the z-transform. Working Paper.

Lu, S. and Jin, Z. (2017). Improved stochastic gradient descent algorithm for svm. *International Journal of Recent Engineering Science (IJRES)*, 4(4):28–31.

Madan, D. B., Carr, P. P., and Chang, E. C. (1998). The variance gamma process and option pricing. *Review of Finance*, 2(1):79–105.

Merrikh-Bayat, F. (2014). Two methods for numerical inversion of the z-transform. *arXiv preprint arXiv:1409.1727*.

Merton, R. C. (1973). Theory of rational option pricing. *The Bell Journal of economics and management science*, pages 141–183.

Nyquist, H. (1928). Certain topics in telegraph transmission theory. *Transactions of the American Institute of Electrical Engineers*, 47(2):617–644.

Persson, P.-O., Franco, M., and Sweeney Blanco, R. (2022). Gradient-based optimization. Accessed: [10-03-2024].

Phelan, C. E. (2018). *Fourier transform methods for the pricing of barrier options and other exotic derivatives*. PhD thesis, UCL (University College London).

Phelan, C. E., Marazzina, D., Fusai, G., and Germano, G. (2019). Hilbert transform, spectral filters and option pricing. *Annals of Operations Research*, 282(1):273–298.

Rajković, P. M., Stanković, M. S., and Marinković, S. D. (2004). A method for numerical evaluating of inverse z-transform. *Facta universitatis-series: Mechanics, Automatic Control and Robotics*, 4(16):133–139.

Ross, S. M. (2014). *Introduction to probability models*. Academic press.

Ruijter, M., Versteegh, M., and Oosterlee, C. W. (2015). On the application of spectral filters in a fourier option pricing technique. *Journal of Computational Finance*, 19(1):75–106.

Schafer, R. W. and Oppenheim, A. V. (1989). *Discrete-time signal processing*, volume 5. Prentice Hall Englewood Cliffs, NJ.

Schmelzer, T. and Trefethen, L. N. (2007). Computing the gamma function using contour integrals and rational approximations. *SIAM Journal on Numerical Analysis*, 45(2):558–571.

Shannon, C. E. (1949). Communication in the presence of noise. *Proceedings of the IRE*, 37(1):10–21.

Tian, Y., Zhang, Y., and Zhang, H. (2023). Recent advances in stochastic gradient descent in deep learning. *Mathematics*, 11(3).

Zeebaree, D. Q., Haron, H., Abdulazeez, A. M., and Zebari, D. A. (2019). Trainable model based on new uniform lbp feature to identify the risk of the breast cancer. In *2019 international conference on advanced science and engineering (ICOASE)*, pages 106–111. IEEE.

Zhang, J. (2019). Gradient descent based optimization algorithms for deep learning models training. *arXiv preprint arXiv:1903.03614*.

Appendices